Graphical Visualization of Vortical Flows by Means of Helicity

Yuval Levy*
Technion, Israel Institute of Technology, Haifa, Israel
David Degani†
NASA Ames Research Center, Moffett Field, California
and
Arnan Seginer‡
Technion, Israel Institute of Technology, Haifa, Israel

Helicity density and normalized helicity are introduced as important tools for the graphical representation of three-dimensional flowfields that contain concentrated vortices. The use of these two quantities filters out the flowfield regions of low vorticity, as well as regions of high vorticity but low speed where the angle between the velocity and vorticity vectors is large (such as in the boundary layer). Their use permits the researcher to identify and accentuate the concentrated vortices, differentiate between primary and secondary vortices, and mark their separation and reattachment lines. The method also allows locating singular points in the flowfield and tracing the vortex-core streamlines that emanate from them.

Nomenclature

H = helicity
H_d = helicity density
H_n = normalized helicity
M_∞ = freestream Mach number
Re_D = Reynolds number
V = velocity
α = angle of attack
ω = vorticity

Introduction

THE supercomputer era has produced solutions of complex three-dimensional compressible viscous flows that could not have been obtained by conventional means. The tremendous computational power (large memory and high computational speed) of modern computers can be applied to the calculation of flowfields over various body shapes by the solution of thin-layer Navier-Stokes equations or even of the full Navier-Stokes equations.

Such solutions (e.g., those obtained by the algorithms described in Refs. 1-4) generate very large data bases. A typical solution will usually yield five quantities (three components of the momentum, density, and energy) per mesh point, on a typical grid of about a million points. The result is several million values per solution for a steady flow, or several million values per time step for an unsteady flow.

A similar situation with experimental data also has developed in recent years with the introduction of laser-Doppler anemometry, which allows measurement of three velocity components at many very closely spaced points in the flowfield, and these as a function of time, as well.

An analysis and understanding of the flowfield by studying that vast information is practically impossible. The researcher has to resort to a graphical representation of the flowfield to distill this information in a way that will furnish him with a grasp of the physics of the flowfield. But care has to be taken to choose the right method, because conventional graphical representation may require more time to generate and analyze than the time needed to generate the numerical results. Furthermore, graphical representations can be ambiguous and may be misleading, as will be shown here. The method to be proposed here is simple and unambiguous.

In the past, most flowfields that were studied were two-dimensional. These were adequately represented by constant-valued contour plots of various scalar quantities, such as density (in compressible flow) and pressure, as well as by streamlines in steady flows, or by velocity vector plots. Most of the methods that are currently used to describe flowfield solutions are simple adaptations or extensions of the same methods. The flowfields are, however, complex three-dimensional fields that are extremely difficult to represent by two-dimensional views.

Among the most complex three-dimensional flowfields are those generated by slender bodies at high angles of attack. These are characterized by the presence of pairs of vortices over their leeward side and in their wake. The vortices, which are highly concentrated in high Reynolds number flows and are more diffused at lower Reynolds numbers, can be observed experimentally by flow-visualization techniques. Also observed are the vortex cores that are characterized by their having local speeds much higher than the ambient speeds and, therefore, also having lower densities when the flow is compressible. The details of such complex flows, whether obtained experimentally or computationally, cannot be represented by conventional graphical methods in a way that will clearly display their true character.

Representation of scalar quantities, such as pressure and density, is relatively simple. They are usually used to describe the flowfield far from the body. Pressure and density plots can identify the cores of concentrated primary vortices in high-speed flows, but are not sufficiently sensitive to identify lower speed phenomena, such as secondary vortices or diffused vortices. A major shortcoming of such representations is that they cannot indicate the sense of swirl of the vortices. As a result, they are unable to differentiate between primary and second-

Received Feb. 13, 1989; revision received June 12, 1989.

*Graduate Student, Faculty of Aeronautical Engineering.
†National Research Council Senior Research Associate. Associate Professor, on leave from Technion IIT, Faculty of Mechanical Engineering. Member AIAA.
‡Professor, Faculty of Aeronautical Engineering. Associate Fellow AIAA.

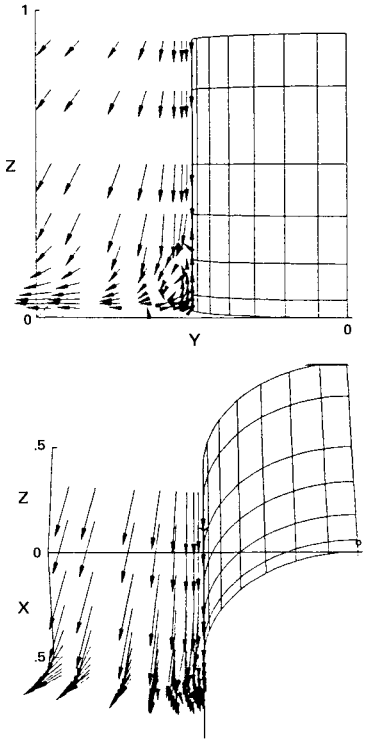

Fig. 1 Two different views of the velocity field near the shoulder of a blunt fin protruding from a flat plate (Ref. 5).

ary vortices, and may give absolutely no information on the vorticity itself. Furthermore, they can be represented only on specific two-dimensional cross sections of the flowfield.

The most important features of the preceding flowfields are vector quantities; namely, the velocity and vorticity fields. One of the best methods to represent two-dimensional flowfields is by means of vectors, i.e., arrows that represent the local velocities by their magnitude and direction. In three-dimensional flows, only projection of the velocity (or vorticity) vectors on a two-dimensional surface (or on a cross section of the flowfield) can be represented. Overlays of several projections will clutter the picture and make interpretation an impossible task. Furthermore, the two-dimensional projection of the flowfield vectors changes with the viewing point and angle, and may be very misleading.[5] Figure 1 (from Ref. 5) demonstrates how changing the viewing angle of the same region of a flowfield can obscure an existing vortex and change the interpretation of the flowfield. This figure shows two different views of the velocity field near the shoulder of a blunt fin protruding from a flat plate. The existence of a vortex core and a separation point is shown very clearly in Fig. 1a. On the other hand, by changing the view angle and the view point (Fig. 1b), the vortex cannot be identified. An additional problem is the choice of the proper cross section of the flowfield that will give the best interpretation of its true character in a two-dimensional projection. This problem is further aggravated at high angles of attack, when the relative angles between the longitudinal axis of the body and the core axes of the vortices are large.

The difficulties in the representation of three-dimensional velocity vector fields are often circumvented by representing the computed surface flow pattern (or the skin friction lines). Plots of the velocity vectors on the limiting surface actually describe the shear lines on the body surface and resemble flow visualizations by the surface oil-flow technique. This technique enables identification of separation and reattachment lines as well as singular points of these lines. These data, with the aid of laws of the topology of the flowfield,[7,8] can give some information on the general character of the flowfield away from the body, but no details such as the presence of singular points above the body that are predicted by the same theories. Information about the flowfield can be expanded by releasing and tracing particle lines from the separation lines that were previously identified. These lines delineate the vorticity layers that are shed by the body and when the layers roll up they outline the vortices, but it is difficult to discern the direction of swirl of the vortices from such plots (Fig. 2). This method does not allow the tracing of streamlines that emanate from the singular points in the flowfield and, therefore, cannot permit a description of the vortex-core streamlines.

In the following, it will be shown that the representations of the helicity density and the normalized helicity, both scalar quantities derived from the velocity, introduce new tools to deal with the problems just described. These representations emphasize the complex parts of the flowfield, identify the vortices, differentiate between primary and secondary vortices, indicate the sense of the swirling motion, locate singular points in the flow, and trace the vortex-core streamlines that emanate from them. To the best of the authors' knowledge, this is the first practical use of helicity-related quantities for the visualization and interpretation of flowfields.

Theoretical Background

In order to represent graphically the preceding vortical flowfields, one has to relate aspects of both the velocity field and the vorticity field (i.e., the curl of the velocity) at the same time. The quantity chosen to do this has to be scalar so that its representation is not complicated by consideration of the viewing angle or cross sections. The interest in concentrated vortices led, naturally, to the choice of quantities that were related to the local vorticity vector. Several scalar quantities were considered. One, for example, was the enstrophy density, which is half the square of the vorticity magnitude. The enstrophy identifies regions of concentrated vorticity, but is not related directly to the velocity, so it cannot distinguish between

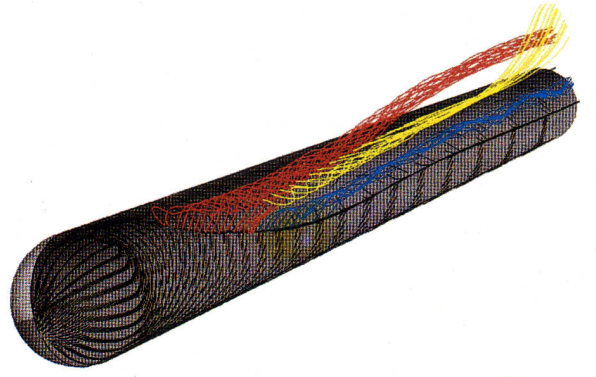

a) Hemisphere-cylinder body; $M_\infty = 1.2$, $\alpha = 19$ deg, $Re_D = 4.45 \times 10^5$

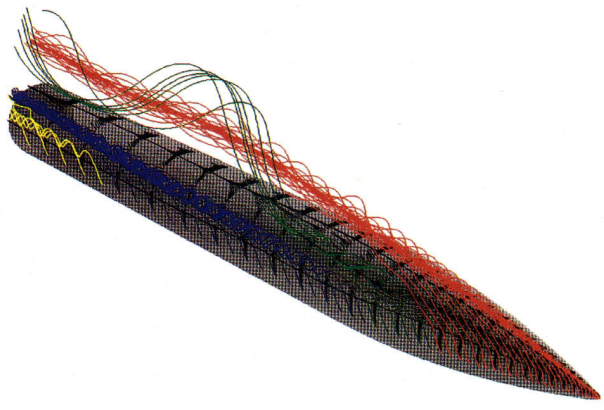

b) Ogive-cylinder body; $M_\infty = 0.2$, $\alpha = 40$ deg, $Re_D = 2 \times 10^5$

Fig. 2 Numerically generated surface shear lines and particle traces.

a boundary layer and a vortex core. Also, because it is always positive, it cannot distinguish between primary and secondary vortices, or indicate their sense of swirl. Only the helicity density and the normalized helicity were found to satisfy those requirements.

Helicity and helicity density were first mentioned in relation to fluid flows by Moffatt,[9] who defined the helicity density as

$$H_d = \boldsymbol{V} \cdot \boldsymbol{\omega} \tag{1}$$

Helicity is defined as the volume integral of the helicity density:

$$H = \int\int\int (\boldsymbol{V} \cdot \boldsymbol{\omega})\, d\bar{v} \tag{2}$$

Moffatt's consideration of helicity was limited to inviscid flow with the vorticity concentrated in two closed vortex filaments with the flow irrotational everywhere else. He used the helicity as a measure of the degree of knottedness of tangled vortex lines. Later studies[10-13] used the so-called "relative helicity," or more properly named, the "normalized helicity,"

$$H_n = \frac{\boldsymbol{V} \cdot \boldsymbol{\omega}}{|\boldsymbol{V}||\boldsymbol{\omega}|} \tag{3}$$

to locate and identify coherent structures in turbulent flows.

The great advantage of helicity density and normalized helicity over other scalar quantities that were described, besides their being simple scalars, is that both their magnitudes and sense are meaningful. High values of helicity density reflect high values of speed and vorticity when the relative angle between them is small. The sign of helicity density is determined by the sign of the cosine of the angle between the velocity and vorticity vectors. Thus, the sign of the helicity density indicates the direction of swirl of the vortex relative to the streamwise velocity component. Both the relative size of the helicity density and the changing of swirl direction, emphasized by graduation in color for magnitude and by different colors for positive or negative values, clearly distinguish between primary and secondary vortices in the graphical representation.

The effectiveness of helicity density as an indicator of vortices is even greater for low subsonic flows, where conventional density mapping is not sufficiently sensitive because density variations are almost negligible. The sensitivity of helicity density remains high because in the core region of a vortex both the velocity and vorticity always reach relatively high values, and the angle between them is small. All of these contribute to high values of the helicity density and to a clear representation of the vortices.

It has just been mentioned that the angle between the velocity and vorticity vectors in the vortex-core regions is small. This means that the normalized helicity, which is the cosine of this angle, will reach its highest absolute numbers in this region. This fact will be used later to locate the vortex axis. Whereas the justification for the use of helicity density and of normalized helicity was up to now quantitative only, the high values of normalized helicity in the core suggest a justification on the basis of theoretical reasoning as well.

Figure 3 (based on Ref. 14) shows the components of the vorticity vector relative to the local streamline. One component is parallel to the local velocity vector and the other two are perpendicular to it. The velocity-oriented component vanishes in two cases: 1) everywhere in a two-dimensional flow, and 2) locally when the flow is two-dimensional, such as on planes of symmetry. Since only this component contributes to the normalized helicity, the latter will be identically zero in two-dimensional flows (where it cannot be used for graphic purposes) and will vanish locally on planes of symmetry, thus emphasizing them in the graphic representation. The other two components of the vorticity do not contribute to the normalized

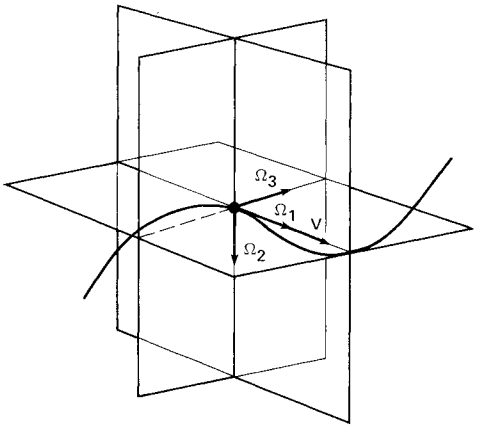

Fig. 3 Vorticity vector components relative to the local streamline (Ref. 14).

helicity, nor to the helicity density, but affect the local curvature of the streamline at the point. Each of these components affects the streamline curvature in the plane that is perpendicular to it and includes the velocity vector. When the two normal components decrease relative to a constant velocity-oriented component, the local curvature of the streamline also decreases. At the same time the angle between the vorticity and velocity vectors also vanishes and the normalized helicity tends toward unity. The magnitude of the normalized helicity is, thus, indicative of the local curvature of the streamlines. In the limiting case, where the velocity and vorticity vectors are parallel, the normalized helicity is exactly equal to unity and the streamline is locally straight. The flow, however, is far from being two-dimensional, because adjacent streamlines are spiraling around this streamline. The fact that the normalized helicity goes to its maximum value on a streamline of minimum curvature will be used later in this paper to locate the vortex-core axis.

Calculations of helicity density and normalized helicity were done in a similar way to the flowfield calculations, by using second-order finite differences in a curvilinear coordinate system; therefore, the accuracy of the raw results was kept intact. The time required for calculations of the preceding quantities was insignificant in comparison to the graphic process time.

Graphical Method

Representative Flowfields

The new method of graphic representation is demonstrated with the numerical results of two flowfield computations:

Case A: A hemisphere-cylinder body (Ref. 15); $M_\infty = 1.2$, $\alpha = 19$ deg, $Re_D = 4.45 \times 10^5$.

Case B: An ogive-cylinder body (Ref. 16); $M_\infty = 0.2$, $\alpha = 40$ deg, $Re_D = 2 \times 10^5$.

The two preceding flowfields are laminar, and the data were generated by three-dimensional solutions of the thin-layer Navier-Stokes equations. In addition to their availability, these flowfield data were chosen to test the new method under different conditions: compressibility effects can be observed in the different Mach number flows; the two different nose shapes generate different types of flow separation, and in case B the flow is unsteady, whereas in case A the flow is steady.

The two different nose shapes were expected to generate different flowfield topologies. The computed surface flow pattern indicated, in both cases (Figs. 2a and 2b), primary and secondary separation lines, as well as reattachment lines. In case A, particles released from the separation lines described two primary vortices with the same sense of rotation and one secondary vortex (Fig. 2a).

The topology of the flowfield can be determined by a study of the surface flow pattern. In case A, several singular points in the surface flow pattern (points where the shear stress vanishes) were observed from the computed surface flow pattern

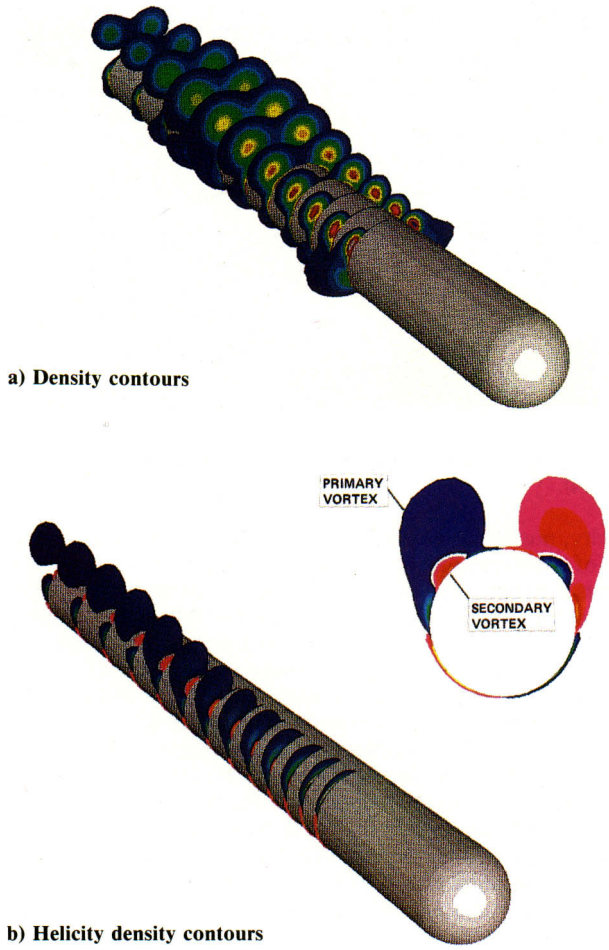

Fig. 4 Contour plots of flowfield around a hemisphere-cylinder body; $M_\infty = 1.2$, $\alpha = 19$ deg, $Re_D = 4.45 \times 10^5$.

of the hemisphere-cylinder body. One of these singular points was a saddle point of separation. This indicates the so-called "closed separation," as defined by Wang.[6] Tobak and Peake[7] preferred to define this type of separation as "global separation." Chapman[8] widened this definition and called the separation where the vortex core emanates from a singular point on the surface as "simple primary separation type II." He also predicted that the hemisphere-cylinder flowfield has an additional singular point above the surface (where the velocity vanishes), and that the vortex core emanates from it. Chapman called this type of separation, "simple primary separation type I."

In case B, although skin-friction lines were observed to converge onto what appeared to be lines of separation, no saddle-type singular points were observed on those lines. We consider that this flow was not really separated. This type of flow was defined by Wang[6] as "open separation," or as "local separation" by Tobak and Peake[7] or by Chapman[8] as "crossflow separation." The vortex cores do not begin at definite points, but are extensions of streamlines that arrive from far upstream. In this case, too, particle lines starting from the separation lines described several primary vortices (Fig. 2b), but secondary vortices could not be identified, although their existence was indicated by the computed surface flow pattern.

Qualitative Flowfield Description by Helicity Density

Before providing a demonstration of the advantages of the proposed method, the flowfields described as cases A and B are represented first by the commonly used mass density contour plots (Figs. 4a and 5a). This is straightforward, because the density is available as part of the solution. In case A, the presence of a lower density in each of the vortex cores identifies the primary vortex and the secondary vortex (Fig. 4a), although with some difficulty, but cannot distinguish between them, nor does it indicate the sense of rotation. In case B, the vortices are weaker and the density gradients are smaller because of the low Mach number and, therefore, the secondary vortices are hardly noticeable (Fig. 5a). The same flowfields are represented again by helicity density plots in Figs. 4b and 5b, respectively. The delineation of the vortices by this method is much clearer. All of the vortices are observable, and the change in sign of the helicity density (and in corresponding color) clearly distinguishes between primary and secondary vortices. This is very clearly seen in the inserts on Figs. 4b and 5b, which are typical cross sections of the flowfields.

The physical understanding of the flowfield can be improved by combining computed surface flow pattern and helicity density plots. The first describes the flow very close to the body, and the latter describes the flow further away. This combination is presented for cases A and B in Figs. 6a and 6b, respectively. The helicity density changes sign across every separation or reattachment line. The transitions from primary to secondary vortex, or vice versa, as well as from attached to separated flow, or vice versa, are emphasized. The excellent agreement between the sign switching of the helicity density and the separation and reattachment lines, as defined by the computed surface flow pattern, validates the proposed method for the representation of the flow not only away from the body, but near the body as well.

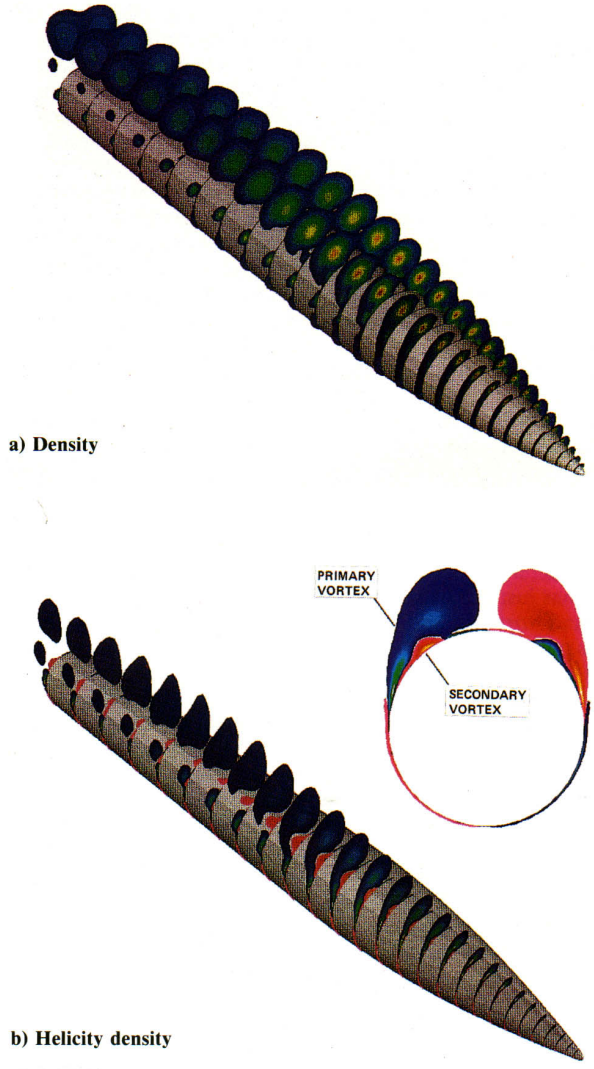

Fig. 5 Contour plots of flowfield around an ogive-cylinder body; $M_\infty = 0.2$, $\alpha = 40$ deg, $Re_D = 2 \times 10^5$.

Core Axis Location by Normalized Helicity

For various reasons—such as comparison between numerical and experimental data, schematic representation of the flowfield, or discretization of the vortical flow for vortex-method computations—researchers are interested in identifying a streamline that is the axis of the vortex core. As mentioned before, in the flowfield topology of case A such a streamline exists, and it begins at a singular point in space above the body. In case B, such a streamline does not exist and the vortex core can be defined only in an asymptotic sense.

Chapman[8] showed that "simple primary separation type I" should have a singular point in the flow above the body. Reference 15 shows a schematic of the off-surface flow of case A and identified such a point (point Q in Fig. 7, taken from Ref. 15), but the exact location of the singular point and the vortex-core streamline that emanates from it were not computed. In principle, if this point could be located accurately and the streamline that passes through it could be found by integration, this would be the vortex-core axis. However, the exact pinpointing of this singular point in the numerical space was practically impossible, even when the computation was done on a high-resolution mesh. Furthermore, the location of the singular point alone would be insufficient and the streamline integration would be impossible because, through a singular point pass more than one streamline and with the velocity there being zero by definition, an integration could not be started.

Trying by any method to locate the vortex core in the flowfield over the fore part of the body would be difficult because of the complexity of the partially developed flow there. On the other hand, the flow over the aft part of the body is more fully developed and, therefore, less complex, and the vortex cores can be identified by most of the graphical methods mentioned before. Observation of this part of the flow shows that the streamlines there are generally less curved than over the fore part. As one approaches the core of the vortex, this curvature is further reduced. Based on the explanation just offered, one can surmise that the angle between the velocity and vorticity vectors is getting smaller and smaller. This leads directly to the conclusion that a flowfield representation by normalized helicity will locate the vortex cores in the regions where the normalized helicity goes toward unity. The points of maximum normalized helicity can be computed at each cross section. These are the points of minimum streamline curvature, and should be on the vortex core axis. An upstream integration (backward integration in time) from such a point located downstream will describe the streamline along the vortex-core axis and should terminate at the singular point.

Figure 8 shows an example of such a computation for case A. It presents normalized helicity contours over the hemisphere-cylinder body with the vortex-core streamline inte-

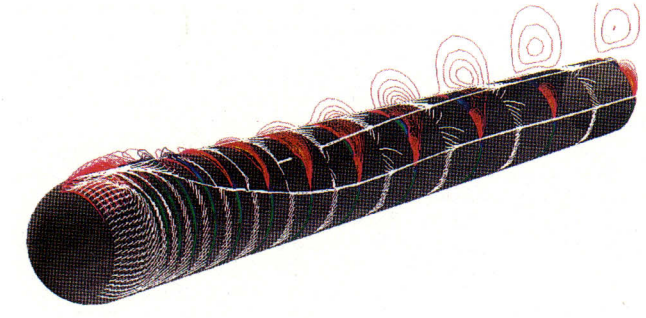

a) Hemisphere-cylinder body; $M_\infty = 1.2$, $\alpha = 19$ deg, $Re_D = 4.45 \times 10^5$

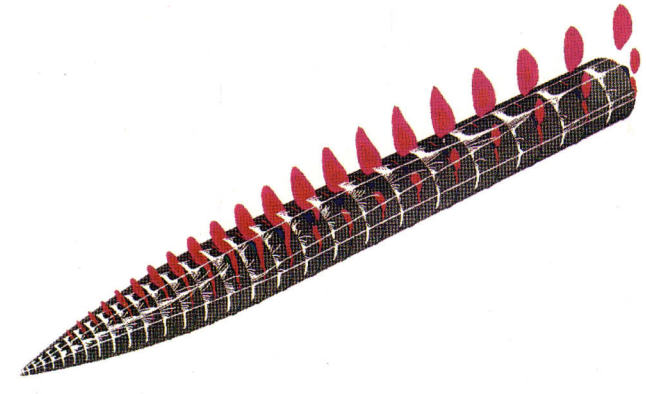

b) Ogive-cylinder body; $M_\infty = 0.2$, $\alpha = 40$ deg, $Re_D = 2 \times 10^5$

Fig. 6 Helicity density contour plots and surface shear lines.

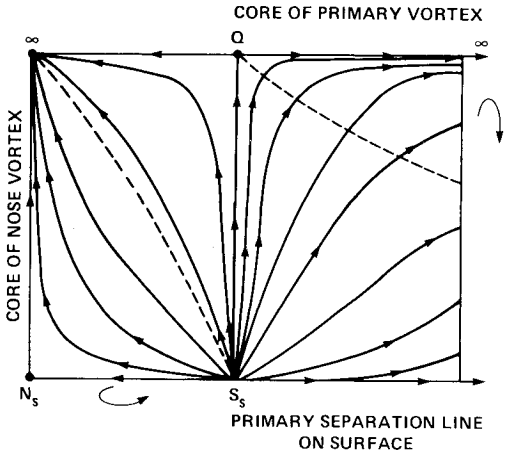

Fig. 7 Unrolled surface of primary separation near nose foci (Ref. 15).

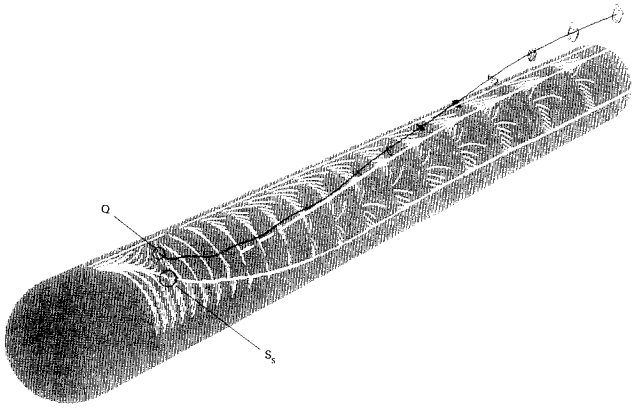

Fig. 8 Normalized helicity contour plots and a vortex-core streamline for a hemisphere-cylinder body; $M_\infty = 1.2$, $\alpha = 19$ deg, $Re_D = 4.45 \times 10^5$.

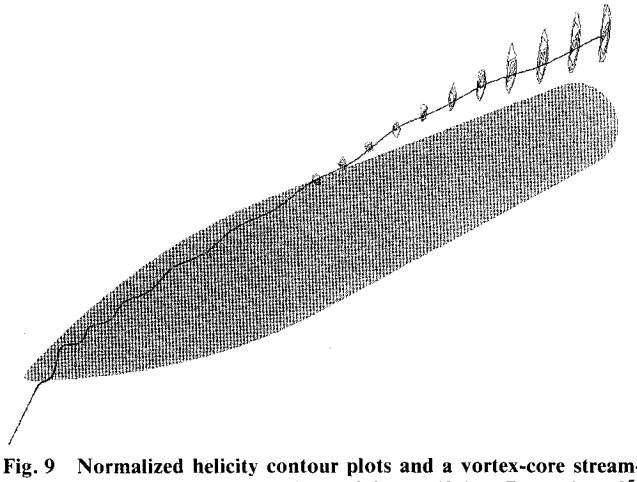

Fig. 9 Normalized helicity contour plots and a vortex-core streamline for an ogive-cylinder body; $M_\infty = 0.2$, $\alpha = 40$ deg, $Re_D = 2 \times 10^5$.

grated upstream from the aft station; and, indeed, it can be seen that in each cross section the line passes through the region of maximum normalized helicity. The values of normalized helicity along the line are very close to unity. The integration of the axis line terminates at a point in space (point Q in Figs. 7 and 8), and the coordinates of this point are 10 grid points above the body surface, practically above the saddle of separation on the surface (point S_s in Figs. 7 and 8). The fact that the computed line is actually the vortex-core axis was verified by releasing several particle lines very close to the starting point of this line. All of the additional lines spiraled around the vortex-core axis.

The "open" or "crossflow separation" of case B does not have the preceding singular points, and the vortex-core axis line can be defined asymptotically only, but the preceding method can still be used. Although the velocity and vorticity vectors in the center of the core are not perfectly aligned in this case, the local curvature of the streamline there is still minimal. Hence, the normalized helicity must reach its maximum value there; therefore, the preceding procedure can be used here as well. Figure 9 shows the results of this procedure, and verifies again that the resulting line passes through the region of maximum normalized helicity of each cross section. As expected, the momentary streamline that describes the vortex axis does not begin at a specific point, but comes from far upstream. Since the flow in case B is unsteady, it seems that the momentary streamline that describes the core axis in unsteady flows follows the same rules as in steady flow, and that at each instant the angle between the velocity and vorticity vectors at the core center is minimal.

Discussion and Conclusions

The preceding results show that the angle between the velocity and vorticity vectors is always minimal in the center of the vortex core, which is the vortex axis. This is in good agreement with several theories. Lewalle[17] shows that equilibrium, or steady-flow conditions, are reached when the flux of normalized helicity is maximal. He obtained this result from the derivation of Ref. 18, which shows that minimum entropy production is a necessary condition for equilibrium and steady state. Reference 12 shows by numerical simulation that in the regions where the angle between the velocity and vorticity vectors is minimal, the energy dissipation also is minimal. This result should be self-evident from Crocco's theorem. Although all of the preceding are integral phenomena (except for Crocco's theorem), there is a reasonable correlation between the preceding conclusions and the fact that the equilibrium vortex-axis position follows the line of minimal angle between the velocity and vorticity vectors. Therefore, the authors propose this line as a definition of the vortex-core axis.

It was shown here that the representation of three-dimensional flowfields that contain concentrated vortices by helicity density curves emphasize the importance and interesting regions of the flowfield. The use of the helicity density filters out the regions of low vorticity (far from the body), as well as regions of high vorticity, but low velocity particularly where the angle between the velocity and vorticity vectors is large (very close to the body in the boundary layer). The method allows distinguishing between primary and secondary vortices, and determining their sense of rotation, while emphasizing the separation and reattachment lines on the body surface. The helicity density plots also present qualitative information on the degree of the concentration of the vortices.

The utilization of normalized helicity identifies the axis of the vortex core, both for closed and open separation. In simple primary separation type I, the singular points above the body, and the streamlines emanating from them that are the vortex-core axes, can be computed by backward integration in time. The same method allows locating the centers of the vortices in open separation. This was based on the fact that the streamline curvature is due to the vorticity components perpendicular to it, which implies that the vortex axes have minimum curvature. This condition is equivalent to the presence of maximum normalized helicity on the vortex axis.

Acknowledgments

This work was supported by NASA Ames Research Center under Grant NAGW-609. The authors would like to thank L. B. Schiff and M. Tobak of NASA Ames Research Center for many useful discussions during the course of this study.

References

[1]Beam, R. M. and Warming, R. F., "An Implicit Finite-Difference Algorithm for Hyperbolic Systems in Conservation Law Form," *Journal of Computational Physics,* Vol. 22, No. 1, Sept. 1976, pp. 87–110.

[2]Steger, J. L., "Implicit Finite Difference Simulation of Flow About Arbitrary Geometries with Application to Airfoils," AIAA Paper 77-665, June 1977.

[3]Beam, R. M. and Warming, R. F., "An Implicit Factored Scheme for the Compressible Navier-Stokes Equations," *AIAA Journal,* Vol. 16, April 1978, pp. 393–402.

[4]Degani, D., "Numerical Algorithm Conjugating Unsteady, Separated, Compressible Flow and a Solid Body Having Arbitrary Distributed Heat Sources," *Numerical Heat Transfer,* Vol. 7, No. 4, Oct.–Dec. 1984, pp. 395–411.

[5]Buning, P. G. and Steger, J. L., "Graphics and Flow Visualizations in Computational Fluid Dynamics," AIAA Paper No. 85-1507-CP, July 1985.

[6]Wang, K. C., "Boundary Layer Over a Blunt Body at High Incidence with an Open Type of Separation," *Proceedings of the Royal Society of London,* Series A, Vol. 34, 1974, pp. 33-35.

[7]Tobak, M. and Peake, D. J., "Topology of Three-Dimensional Separated Flows," *Annual Review of Fluid Mechanics,* Vol 14, 1982, pp. 61-85.

[8]Chapman, G. T., "Topological Classification of Flow Separation on Three-dimensional Bodies," AIAA Paper 86-0485, Jan. 1986.

[9]Moffatt, H. K., "The Degree of Knottedness of Tangled Vortex Lines," *Journal of Fluid Mechanics,* Vol. 35, Part I, Jan. 1969, pp. 117–129.

[10]Levich, E. and Tsinober, A., "On The Role of Helical Structures in Three-Dimensional Turbulent Flow," *Physics Letters,* Vol. 93A, No. 6, Jan. 1983, pp. 293–324.

[11]Tsinober, A. and Levich, E., "On the Helical Nature of Three-Dimensional Coherent Structures in Turbulent Flows," *Physics Letters,* Vol. 99A, No. 6–7, Dec. 1983, pp. 321–324.

[12]Shtilman, L., Levich, E., Orszag, S. A., Pelz, R. B., and Tsinober, A., "On The Role of Helicity In Complex Fluid Flows," *Physics Letters,* Vol. 113A, No. 1, Nov. 1985, pp. 32–37.

[13]Pelz, R. B., Shtilman, L., and Tsinober, A., "The Helical Nature of Unforced Turbulent Flows," *Physics of Fluids,* Vol. 29, No. 11, Nov. 1986, pp. 3506–3508.

[14]Faux, I. D. and Pratt, M. J., *Computational Geometry for Design and Manufacture,* Ellis Horwood Limited, UK, 1979, p. 100.

[15]Ying, S. X., Schiff, L. B., and Steger, J. L., "A Numerical Study of Three-Dimensional Separated Flow Past a Hemisphere-Cylinder," AIAA Paper 87-1207, June 1987.

[16]Degani, D. and Schiff, L. B., "Numerical Simulation of Asymmetric Vortex Flows Occurring on Bodies of Revolution at Large Incidence," AIAA Paper 87-2628, Aug. 1987.

[17]Lewalle, J., "On a Variational Property of Helicity in Incompressible Flows," *Physics Letters A,* Vol. 122, No. 6–7, June 1987, pp. 338–340.

[18]Glansdorf, P. and Prigogine, I., "On a General Evolution Criterion in Macroscopic Physics," *Physica,* Vol. 30, No. 2, Feb. 1964, pp. 351–374.